

The Influence of H₂O Pressure Broadening in High Metallicity Exoplanet Atmospheres

EHSAN GHARIB-NEZHAD¹ AND MICHAEL R. LINE²

¹*School of Molecular Sciences, Arizona State University, Tempe, AZ 85287, USA.*

²*School of Earth and Space Exploration, Arizona State University, Tempe, AZ 85287, USA.*

ABSTRACT

Planet formation models suggest broad compositional diversity in the sub-Neptune/super-Earth regime, with a high likelihood for large atmospheric metal content ($\geq 100 \times$ Solar). With this comes the prevalence of numerous plausible bulk atmospheric constituents including N₂, CO₂, H₂O, CO, and CH₄. Given this compositional diversity there is a critical need to investigate the influence of the background gas on the broadening of the molecular absorption cross sections and the subsequent influence on observed spectra. This broadening can become significant and the common H₂/He or “air” broadening assumptions are no longer appropriate. In this work we investigate the role of water self broadening on the emission and transmission spectra as well as on the vertical energy balance in representative sub-Neptune/super-Earth atmospheres. We find that the choice of the broadener species can result in a 10 – 100 parts-per-million difference in the observed transmission and emission spectra and can significantly alter the 1-dimensional vertical temperature structure of the atmosphere. Choosing the correct background broadener is critical to the proper modeling and interpretation of transit spectra observations in high metallicity regimes, especially in the era of higher precision telescopes such as JWST.

Keywords: planets and satellites: atmospheres, planets and satellites: composition, molecular data

1. INTRODUCTION

A primary goal of exoplanet science is the determination of basic planetary conditions. Transit spectrophotometry observations of planetary atmospheres offer a window into fundamental quantities such as climate and composition (e.g., Madhusudhan et al. (2016)). Determining atmospheric composition is a necessary requirement for assessing the relative importance of various chemical processes (Moses 2014) and greatly assists in understanding planet formation by linking volatile inventory to proto-planetary disk processes (Pollack et al. 1996; Öberg et al. 2011; Madhusudhan et al. 2014; Cridland et al. 2016; Öberg et al. 2011; Mordasini et al. 2016).

One of the key findings of the Kepler Mission (Borucki et al. 1997) is that a majority of exoplanets fall within this “warm sub-Neptune” regime ($\sim 2\text{--}4$ Earth radius, $T < 1000$ K) (Fressin et al. 2013; Batalha 2014; Fulton et al. 2017). These planets have been an intense area of focus for transit spectra observations with the Hubble Space Telescope (HST) (Kreidberg et al. 2014a; Fraine et al. 2014; Knutson et al. 2014). In addition, over the next decade they will serve as the link between jovian worlds and terrestrial planets as well as being the most prolific population of planets to be found by the Transit-

ing Exoplanet Explorer Satellite (TESS, Sullivan et al. (2015); Louie et al. (2018); Barclay et al. (2018); Kempton et al. (2018)).

Planet formation, interior structure, and atmospheric chemistry modeling (Fortney et al. 2013; Moses et al. 2013; Lopez & Fortney 2014) suggest extreme compositional diversity within this sub-population, with a high likelihood for large atmospheric metallicities ($> 100 \times$ Solar). Given this potential for compositional diversity, the assumption of “jovian-like” H₂/He-dominated atmospheres may not always be appropriate. Instead, with currently measured atmospheric metallicities reaching as high as $\sim 300\text{--}1000 \times$ solar (Line et al. 2014; Fraine et al. 2014; Kreidberg et al. 2014b; Knutson et al. 2014; Morley et al. 2017), molecules such as H₂O and CO₂ will become the dominant bulk constituents (Moses et al. 2013; Hu & Seager 2014).

Along with this diversity in composition, comes with it numerous challenges in atmospheric modeling, which ranges from chemical modeling (Hu & Seager 2014) to cloud microphysics (Ohno & Okuzumi 2018) to 3D climate modeling (Kataria et al. 2014). Nearly all flavors of atmospheric modeling that aim to make observational predictions require radiative transfer computations. A key necessary ingredient in radiative transfer computa-

tions are the opacities, which for planets, are dominated by the molecular absorption cross sections (hereafter, ACS (Mihalas 1970)). The ACS of a given molecule typically consist of billions of lines representing the ability of a molecule to absorb or emit photons. Each line has its own linewidth (or broadening) typically specified through the degree of thermal/Doppler and pressure broadening (Goody & Yung 1995). Pressure broadening is the net cumulative effect of interactions between the absorbing molecule in question (e.g., H₂O) and with its neighboring molecules (or bath gases, e.g., H₂, He) or by self broadening (H₂O with itself). Much exo-atmospheric relevant ACS focus, specifically broadening, has been jovian-centric (e.g., H₂/He dominated compositions and broadening Freedman et al. (2008); Tennyson et al. (2016); Grimm & Heng (2015); Hedges & Madhusudhan (2016)) which had been largely driven by the abundance of high fidelity “hot-Jupiter” observations and carry over from brown dwarf modeling.

Exploration of pressure broadening assumptions in exo-atmospheres is not new (e.g., Grimm & Heng (2015); Hedges & Madhusudhan (2016)). Hedges & Madhusudhan (2016) provide a comprehensive overview of the various pressure broadening effects including resolution, line-wing cutoff, Doppler versus pressure, and more relevant to our investigation, an initial look at the impact of a broadener choice. They too explore the impact of H₂O versus H₂ broadening on the H₂O ACS, specifically over HST wavelengths, and found that the band-averaged ACS can change up to an order-of-magnitude.

In this letter we expand upon the work in Hedges & Madhusudhan (2016) to not only determine the influence of H₂O self broadening on the H₂O ACS, but also as a function of water fraction, and more importantly we quantitatively assess the integrated effect that the broadener choice has on the *observable spectra* as well as on the impact on the atmospheric vertical energy balance. This work is crucial to the proper interpretation of transit spectra observations in high metallicity regimes, expected of the sub-Neptune/Super-Earth population. In §2 we describe our data sources and how we compute the ACS and the transmission/emission spectrum and self-consistent modeling approach. In §3 we compare the impact of H₂O self broadening with the standard H₂/He broadening assumption. Finally, in §4 we discuss the implications and future prospects. We also make our newly computed water ACS grid for both broadeners publically available¹.

2. METHODS

In this initial investigation on the impact of *non*-H₂/He foreign broadening on transmission/emission spectra, we choose to focus on H₂O because: 1) H₂O is the most prominent absorber in exoplanet spectra due to its large abundance over a range of elemental compositions (Moses et al. 2013) and multiple strong absorption bands from the optical to far infrared wavelengths and 2) it shows the largest sensitivity to choice of broadener when compared to other species (a factor of ~ 7 increase in broadening when compared to H₂/He, Table 1).

Table 1. Lorentzian half-width coefficients γ_L [cm⁻¹/bar] for relevant broadeners. The focus of this work is on influence H₂O self and H₂/He broadening on the H₂O absorption cross sections (bold).

Absorber	Broadener	γ_L	$\frac{H_2/He}{\gamma_L} \dagger$	Ref.
H ₂ O	Self $\dagger\dagger$	0.3 – 0.54	7×	1,2
	H₂/He *	0.05 – 0.08	1×	1
	CO ₂	0.15 – 0.20	3×	1
	air	0.08 – 0.1	1.5×	1
CH ₄	Self	0.06 – 0.09	1.5×	3
	H ₂ /He	0.05 – 0.08	1×	4
	H ₂ O	0.06 – 0.09	1.5×	5
	CO ₂	0.07 – 0.09	1.5×	6
	air	0.02 – 0.07	1×	3
CO ₂	Self	0.08 – 0.12	2×	7
	H ₂ /He	0.09 – 0.12	2×	8
	H ₂ O	0.10 – 0.14	2.5×	9
	air	0.05 – 0.08	1×	7
CO	Self	0.04 – 0.09	1×	10
	H ₂ /He	0.04 – 0.08	1×	10
	H ₂ O	0.07 – 0.1	1.5×	11
	CO ₂	0.07 – 0.1	1.5×	11
	air	0.05 – 0.07	1×	12

[†] Relative to the average value of γ_L of H₂O@[H₂+He].

^{††} Denoted by H₂O@[self] in the text and figures.

* Denoted by H₂O@[H₂+He] in the text and figures.

Refs.: ¹ (Brown et al. 2005), ² (Ptashnik et al. 2016), ³ (Smith et al. 2014), ⁴ (Pine & Gabard 2003), ⁵ (Delahaye et al. 2016a), ⁶ (Lyulin et al. 2014), ⁷ (Devi et al. 2016), ⁸ (Padmanabhan et al. 2014), ⁹ (Delahaye et al. 2016b), ¹⁰ (Devi et al. 2002), ¹¹ (Hartmann et al. 1988), ¹² (Devi et al. 2012), and also data extracted from Refs. in Table 3 of (Hartmann et al. 2018) and from (Gordon et al. 2017).

The fundamental approach here is to compute the H₂O ACS being under different end-member scenarios, with the first the standard “Jovian-like” H₂/He broadening (H₂O@[H₂+He]) and the second, pure H₂O broadening (H₂O@[self]), which would be more appropriate for high metallicity or all steam atmospheres. We would then like to determine the spectral differences between H₂/He and self broadening of H₂O in high metallicity/all steam atmospheres.

2.1. Line Lists

¹ LINK:TBD UPON ACCEPTANCE

In order to generate the pressure-broadened H₂O ACS, the completeness and the accuracy of line lists and pressure coefficients data are essential. These can be determined either through high-level quantum mechanics calculations or through spectroscopic laboratory measurements. The EXOMOL database contains the complete water BT2 line list (Barber et al. 2006) for $T \leq 3000\text{K}$, rotational quantum numbers (J) up to 50 and frequencies up to $30,000\text{ cm}^{-1}$; a trimmed version of this linelist is used in the HITEMP database (Rothman et al. 2010). The NASA AMES line list (Partridge & Schwenke 1997) is another ab-initio source of water data which has more accurate line positions than BT2 but less complete. Recently, there has been an attempt to improve the BT2 linelist by refining the potential energy surfaces which resulted in raising J up to 72 and frequencies up to $40,000\text{ cm}^{-1}$ (Polyansky et al. 2016). The pressure-broadening data provided by EXOMOL are limited to H₂ and He. Complimentary to ab initio studies, laboratory data integrated into the HITRAN database (Rothman et al. 1998) leverages high-resolution spectrometers to provide precision line positions and intensities. Experimental ACS data are mostly limited to the earth-like environmental conditions (i.e., $T < 350\text{K}$, $P < 1\text{ bar}$) with the dominant background broadener being “air” (N₂/O₂).

There is a clear gap in exoplanet relevant ACS, lying between the low temperature air broadening provided by HITRAN (applicable to temperature terrestrial planetary atmospheres), and the high temperature H₂/He broadening given by HITEMP (applicable to H/He dominated Jovian-like worlds). The high metallicity warm-(sub)Neptune/Supe-Earth sub population of exoplanets occupies a compositional regime between these two: neither pure H₂/He nor pure “air”. In order to fill this gap we generate an H₂O@[H₂+He] and H₂O@[self] ACS database. We leverage the readily available EXOMOL (Tennyson et al. 2016) line-list data which provides the full BT2 line list (Barber et al. 2006) up to 3000K , $J \leq 50$ and energies up to $30,000\text{ cm}^{-1}$; valid over a broad range of “typical” exoplanet environmental conditions.

2.2. Computation of pressure-broadened H₂¹⁶O absorption cross sections

Molecules in the outermost layer of a given atmosphere (where $P < 10^{-6}\text{ bar}$) experience a negligible amount of interactions with their neighboring atoms or molecules due to the low collisional frequency and large collisional frequency (see results section by (Lyons et al. 2018)). In this environment, Doppler broadening will be the dominant effect which forms the spectral line shape and will depend on the molecular mass, temperature,

and spectral line position. Absorbing molecules start to collide and interact with background molecules more frequently as pressure increases in the lower layers in the atmosphere. These pressure broadening interactions will increase as the pressure goes above $\sim 10^{-4}\text{ bar}$, and will become the dominant broadening effect at $P > 10^{-1}\text{ bar}$. The pressure broadening line profile can be represented effectively through Lorentzian line shape and the associated Lorentzian linewidth Γ_L will be calculated through Eq. (1):

$$\Gamma_L = \sum_b (T/T_{ref})^{-n_T^b} \gamma_L^b P_b \quad (1)$$

where Γ_L^b is the Lorentzian coefficient, P_b is the broadeners partial pressure, T_{ref} is the reference temperature (i.e., 296K), n_T^b is the temperature-dependence coefficient, and index b represents the dependency of these parameters into the broadener (Hedges & Madhusudan 2016). Kinetic theory predicts the $n_T^b = 0.5$. In a typical broadened ACS spectra, both Doppler- and pressure-broadening line profiles convolve to generate Voigt profile, and the Voigt linewidth Γ_V (Olivero & Longbothum 1977) is represented with Eq. (2):

$$\Gamma_V = 0.5346 \Gamma_L \sqrt{0.2166 \Gamma_L^2 + \Gamma_G^2} \quad (2)$$

where Γ_G is the Doppler linewidth. In this study, the pressure-broadened H₂O ACS data are computed for two set of broadeners: 1) 85% H₂ and 15% He using pressure coefficients data presented by EXOMOL group (Barton et al. 2017), and 2) 100% H₂O using the average value of available experimental self broadening coefficients as J-independent data. The water BT2 linelist (Barber et al. 2006) is inputted into the EXOCROSS script² (Yurchenko et al. 2018) to model the full Voigt profile (Humlíček 1979) of every single line between $100\text{--}30,000\text{ cm}^{-1}$ over a grid of applicable temperatures and pressures (Table 2). The spectral sampling resolution is optimized as a function of temperature, pressure, and spectral sub-divisions in such a way as to fully resolve the individual lines without undue computational burden (Table 2). Figure 1 illustrates the comparison between our adaptive resolution (see Table 2 i.e. 1 sampling point per half width: $1/\Gamma_V$ or 2 sampling points per half width: $2/\Gamma_V$) with ultra high sampling of 6 points per half width ($6/\Gamma_V$) and with the EXOMOL computed ACS³ for H₂O@[H₂+He] for $P = 10^{-3}\text{ bar}$ and $T = 400\text{K}$.

² <https://github.com/Trovemaster/exocross>

³ <http://exomol.com/data/data-types/xsec/H2O/1H2-16O/BT2/>

The H_2O ACS are computed for two sets of broadeners: 1) 85% H_2 and 15% He using the J-dependent pressure coefficients from EXOMOL (Barton et al. 2017), and 2) 100% H_2O using the average value of available experimental self broadening coefficients (Ptashnik et al. 2016).

Table 2. Grid and computational assumptions over which the H_2^{16}O cross sections are computed. There are 270 T-P combinations and two broadener choices (H_2+He versus H_2O). A variable wavenumber resolution is chosen to properly sample the Voigt-widths at each given T-P pair. Finer sampling results in negligible differences in the ACS.

ACS	Case 1:	85% H_2	15% He			
	Case 2:	100% H_2O				
T(K)	400 900	425 1000	475 1100	500 1200	575 1300	650 725 800 1400 1500
P(bar)	10^{-6} 10^{-3} 1	3×10^{-6} 3×10^{-3} 3	10^{-5} 10^{-2} 10	3×10^{-5} 3×10^{-2} 30	10^{-4} 10^{-1} 100	3×10^{-4} 3×10^{-1} 300
Resolution*	100 1000	– –	1000 30000	cm^{-1} cm^{-1}	: :	$1/\Gamma_V$ $2/\Gamma_V$
Line wing cut-off†		$P > 1$ $P \leq 1$	bar: bar:	300 100	cm^{-1} cm^{-1}	

† The Lorentz wing shape may not be appropriate out at such distances (Freedman et al. 2008)

2.3. Modeling the Impact on Transmission/Emission Spectra of Transiting Exoplanets

To assess the significance of the broadener assumption on exoplanet transmission/emission spectra, we use the CHIMERA (Line et al. 2013, 2014; Stevenson et al. 2014; Kreidberg et al. 2015; Line & Parmentier 2016; Kreidberg et al. 2018) code with our newly generated ACS (converted to $\lambda/\Delta\lambda=100$ correlated-K coefficients (Amundsen et al. 2016)) to model transit/eclipse spectra of a representative sub-Neptune like planet (GJ1214b (Harpsoe et al. 2013), $T_{eq}=500\text{--}900\text{K}$). We first generate forward model spectra using both sets of ACS ($\text{H}_2\text{O}@\text{[self]}$ and $\text{H}_2\text{O}@\text{[H}_2+\text{He}]$) given a fixed temperature-pressure profile (TP, Guillot (2010) Eqs. 24, 49)⁴ and either 100% H_2O or 500×Solar metallicity assuming thermochemical equilibrium molecular abundances⁵. Second, we compute a self-consistent radiative equilibrium atmosphere⁶ using the tools described in Ar-

⁴ With $\kappa_{th} = 3 \times 10^{-2} \text{ cm}^2/\text{g}$, $\gamma = 0.1$, $T_{eq}=500, 700, 900\text{K}$, $T_{int}=0\text{K}$

⁵ NASA CEA2 (Gordon & McBride 1994) with scaled solar (Lodders et al. 2009) abundances. We include as opacities in this scenario H_2/He broadened H_2O , CH_4 , CO , CO_2 , NH_3 , H_2S , Na ,

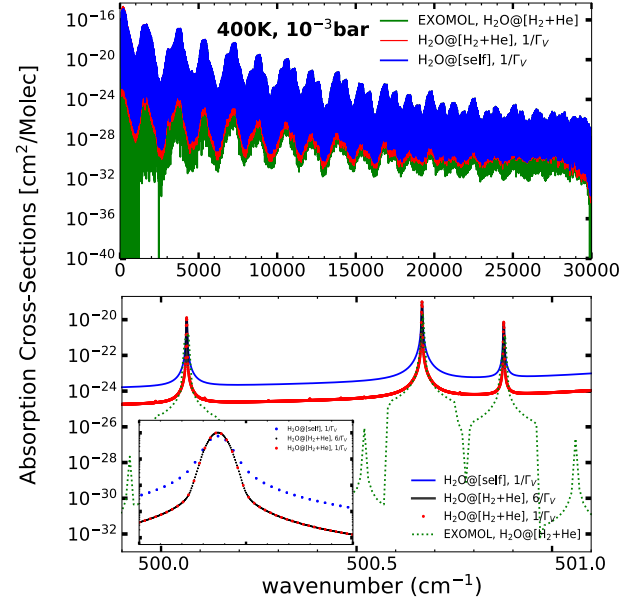


Figure 1. Computed absorption cross sections generated at 1 mbar, 400K comparing $@\text{[self]}$ (Blue) and $@\text{[H}_2+\text{He}]$ (red) broadening with the EXOMOL $@\text{[H}_2+\text{He}]$ (green) broadened spectra. The top panel shows the full spectral range at this T-P combination. The bottom panel shows a zoom in around 500 cm^{-1} , and a further zoom in in the inset in order to illustrate the influence of the computational sampling resolution and to compare with the EXOMOL pre-computed cross sections. Our coarsest sampling resolution ($1/\Gamma_V$, red and blue dots) is high enough to adequately represent lines (when compared to the $6/\Gamma_V$ used in Hedges & Madhusudhan (2016)) at these low pressures, temperatures, and wavenumbers. Our line-wing cutoff is sufficiently large. Differences in sampling resolution are negligible when compared to the influence of the broadener.

cangeli et al. (2018); Mansfield et al. (2018); Kreidberg et al. (2018) to determine the impact of water broadening on the vertical energy balance and, in turn, on the observed spectra. We discuss our findings in the next section.

3. RESULTS

3.1. Impact on Cross Sections

Figure 2 illustrates the effect of temperature, pressure, and water abundance on the difference between $@\text{[self]}$ and $@\text{[H}_2+\text{He}]$ broadened ACS near $6 \mu\text{m}$. The top panel shows how broadening changes with temperature

K, HCN , C_2H_2 , TiO , VO , PH_3 , and H_2 H_2/He CIA (Freedman et al. 2014)

⁶ Zero internal heat flux, PHOENIX stellar model for GJ1214, and an equilibrium temperature of 550 K so as to keep temperatures at all layers within the valid cross section temperature range of 400–1500K

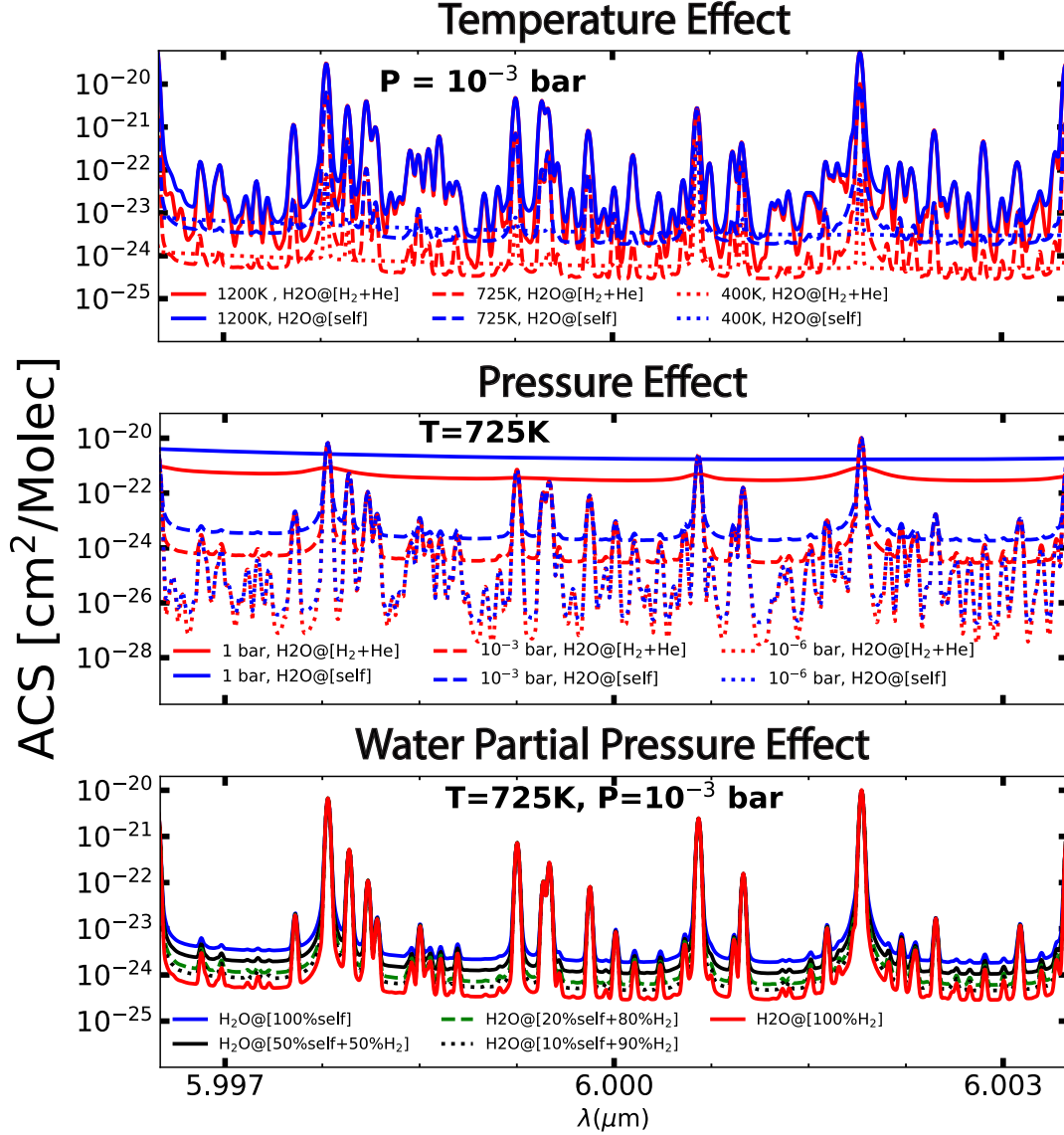


Figure 2. Illustration of the impact of @[self] (blue) versus @[H₂+He] (red) on the absorption cross sections near 6 μ m. The top panel shows the influence of temperature on the broadening difference at a fixed representative pressure of 1 mbar. At 1200K (1 mbar) the lines are purely Doppler broadened resulting in little effect. The middle panel shows the influence of pressure at a fixed temperature. The Doppler cores are negligible by 1 bar. The bottom panel shows the impact of the relative weighting of self versus H₂ broadening (e.g., composition dependence) at a fixed temperature and pressure. Absorption cross section differences are largest in the pressure-broadened line wings, with pure @[self] typically 1 order of magnitude larger. A factor of 5 in broadening difference occurs by the time the relative abundance of water reaches $\sim 30\%$. In general, @[self] broadening becomes more important at higher pressures, cooler temperatures, and longer wavelengths due to the increased prominence of pressure broadening over Doppler broadening.

at a fixed pressure of 1 mbar. Differences are largest for cooler temperatures where pressure broadening becomes more important. The middle panel illustrates the impact of different pressures at a fixed temperature (725K). Even at low pressures (1 μ bar) pressure broadening differences are still present in the line wings. The bottom panel shows the effect of varying water abundance on the combined @[self]+@[H₂] broadening at a

fixed temperature and pressure (725K, 1 mbar). With pure self broadening, differences in the line wings can approach an order of magnitude. For a $\sim 30\%$ mole fraction of water, the ACS is about 3–5 \times greater than pure hydrogen broadening. While not shown, these differences become larger at longer wavelengths and smaller at shorter wavelengths due to the relative importance of Doppler-to-pressure broadening.

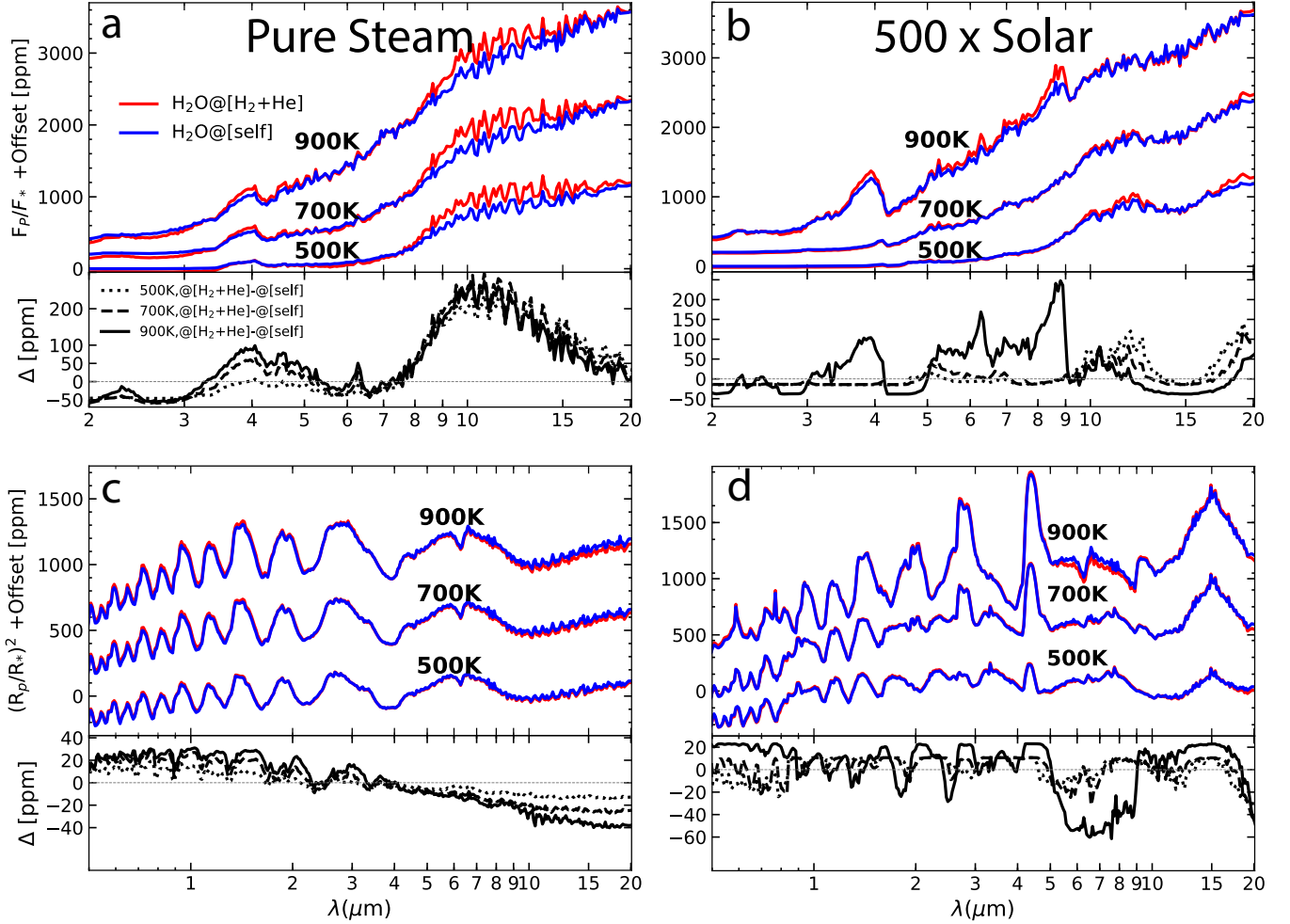


Figure 3. Effect of water self broadening (@[self], blue) compared to the standard H₂/He broadening (@[H₂+He], red) on pure steam (left column: a,c) and high metallicity (500× solar-right column: b,d) atmospheres with equilibrium temperatures of 500, 700, and 900K. The top row (a,b) compares emission spectra and the bottom row shows relative transmission spectrum differences (c,d). The bottom panel in each shows the relative spectral difference (Δ). Differences range anywhere from a few 10s to a few 100s of ppm and show a strong wavelength dependence.

3.2. Direct Impact on Transmission/Emission Spectra

More practically, Figure 3 summarizes the key impact of @[H₂+He] versus @[self] broadening on the emission (top row) and transmission (bottom row) spectra of a typical sub-Neptune under the assumption of a pure steam atmosphere (left column) and a 500×Solar metallicity⁷ scenario (right column). Overall, we find that the differences (Δ [ppm]) in the bottom panels in Figure 3a,b,c, and d) are quite large, 10s to 100s of ppm. These differences are well within the detectable range of both HST (Kreidberg et al. 2014a), and certainly the

James Webb Space Telescope (JWST, e.g., Greene et al. (2016); Bean et al. (2018)), especially for the anticipated windfall of such planets around bright stars (Sullivan et al. 2015).

In the all-steam atmospheres, emission differences (Figure 3a) are largest in the window regions ($\sim 4\mu\text{m}$, $\sim 10\mu\text{m}$). The increased flux for the @[H₂+He] broadened ACS is because of the lower opacity, permitting flux from deeper, hotter layers to emerge (for a fixed TP). The increased opacity due to the @[self] broadening obscures the deeper/hotter layers, resulting in lowered fluxes at those wavelengths. These differences are, of course, strongly dependent upon the temperature structure within the atmosphere. As these spectra assume a fixed TP there is a difference in net radiated flux, which will most certainly have an influence on the radia-

⁷ While the water mixing ratio is only ~ 10 – 20% for these conditions, we still use the pure @[self]-broadened water ACS as it is still a more accurate approximation than pure @[H₂+He] broadening

tive balance and thermal structure in the atmosphere, as discussed in §3.3.

Transmission spectra tell a similar, albeit less dramatic story with relative differences of ~ 60 ppm across shown wavelength range. The “linear-like” slope in the differences with wavelength is due to the frequency dependence of Doppler-to-pressure broadening.

The effects at high metallicity ($500\times$ Solar, Figure 3, right column) are less extreme (10’s of ppm) due to the reduced abundance of H₂O (10 – 20%) and the significant abundances of additional opacity sources (mainly CO₂, CO, CH₄, and H₂/He). Furthermore, due to the reduced impact of H₂O@[self] broadening (Figure 2), we expect an approximate (comparing 1 mbar line wings) reduction of $3\text{--}5\times$ to $\sim < 10$ ppm in the transmission spectra.

3.3. Impact on Self-Consistent 1D Atmosphere

Figure 4 shows the impact of self broadening on the 1D radiative balance (and subsequent observational effects) of a ~ 550 K planet under the all steam and $500\times$ Solar scenarios. The @[self] broadening results in $\sim 100\text{--}180$ K hotter temperatures below the ~ 1 mbar level and ~ 60 K cooler above for the all steam scenario (Figure 4a). More intuitively, the increased @[self] mean opacity “shifts” the averaged thermal “ $\tau=1$ ” level to a $\sim 3\times$ lower pressure in the all steam scenario. This shift is readily seen in the band averaged contribution functions (Figure 4a). A similar, but lesser, effect is seen in the $500\times$ Solar metallicity scenario (up to ~ 70 K) because the water abundance is lower by a factor of ~ 5 (Figure 4b). The radiative response of the TP to the integrated flux differences (up to 40% for steam and 10% for $500\times$ Solar, green versus red curves in Figure 4c,d) between the @[self] versus @[H₂+He] acts to reduce the emission spectrum differences, however, to a still detectable 10s of ppm (Figure 4c,d).

The transmission spectra (Figure 4e,f) show comparable differences (30–40 ppm) to the 500 K scenario from Figure 3c,d. However, there are now two effects taking place that create the transmission differences. The first is the scale height effect due to the differences in the TP (@[H₂+He]-@[self], H₂O TP), and the second, as before, is the broadening difference. Both effects contribute equally to the overall differences in the transmission spectra. Despite the self-consistent adjustment of the TP, differences in both emission and transmission are still above detectable levels (10’s of ppm)

4. CONCLUSIONS

The aim of this work is to determine the observable impact of molecular pressure broadening under differ-

ent plausible bulk atmospheric compositions likely representative of the Super-Earth/(sub)Neptune planetary regime. Specifically, we focused on the differences between the typically assumed H₂/He broadening and water self broadening on the water vapor absorption cross sections. From our analysis we arrive at the following key points:

- Absorption cross section differences between water self and the standard assumed H₂/He broadening are up to an order of magnitude in the pressure broadened line wings (similar to [Hedges & Madhusudhan \(2016\)](#)), and is noticeable over a range of applicable temperatures and pressures.
- The influence of self broadening is composition dependent and non-linear, with \sim half of the difference achieved by water mole fractions of $\sim 30\%$ for a representative temperature and pressure.
- Transmission and emission spectra differences for representative sub-Neptune atmospheres range between a few 10’s of ppm up to 100’s of ppm, depending upon wavelength, temperature, and water abundance. These differences are not negligible considering currently achieved HST precisions of ~ 15 ppm and possible precisions as low as a few ppm for JWST. Differences will vary depending upon additional parameters like temperature gradient (for emission), planet-to-star radius ratio, and scale height.
- The assumption of water self broadening (or lack thereof) can have a significant impact on the 1D vertical energy balance, with temperature differences of up to 180K in pure steam atmospheres (or a half-a-decade lower pressure shift in the emission levels) and 10’s of K in high metallicity atmospheres.

This work is certainly not an exhaustive exploration of all possible broadening (Table 1) or planetary atmosphere conditions. However, it serves to illustrate that the broadener composition can have a non-negligible impact on the observables and continues to illustrate the importance and key role of laboratory data on planetary atmosphere modeling. ([Fortney et al. 2016](#))

5. ACKNOWLEDGEMENTS

EGN and MRL thank J. Lyons, A. Heays, R. Freedman, M. Marley, J. Fortney, P. Mollière, L. Pino and the Arizona State University exoplanet group for many useful discussions. We especially thank S. Yurchenko for invaluable assistance with the EXOCROSS code,

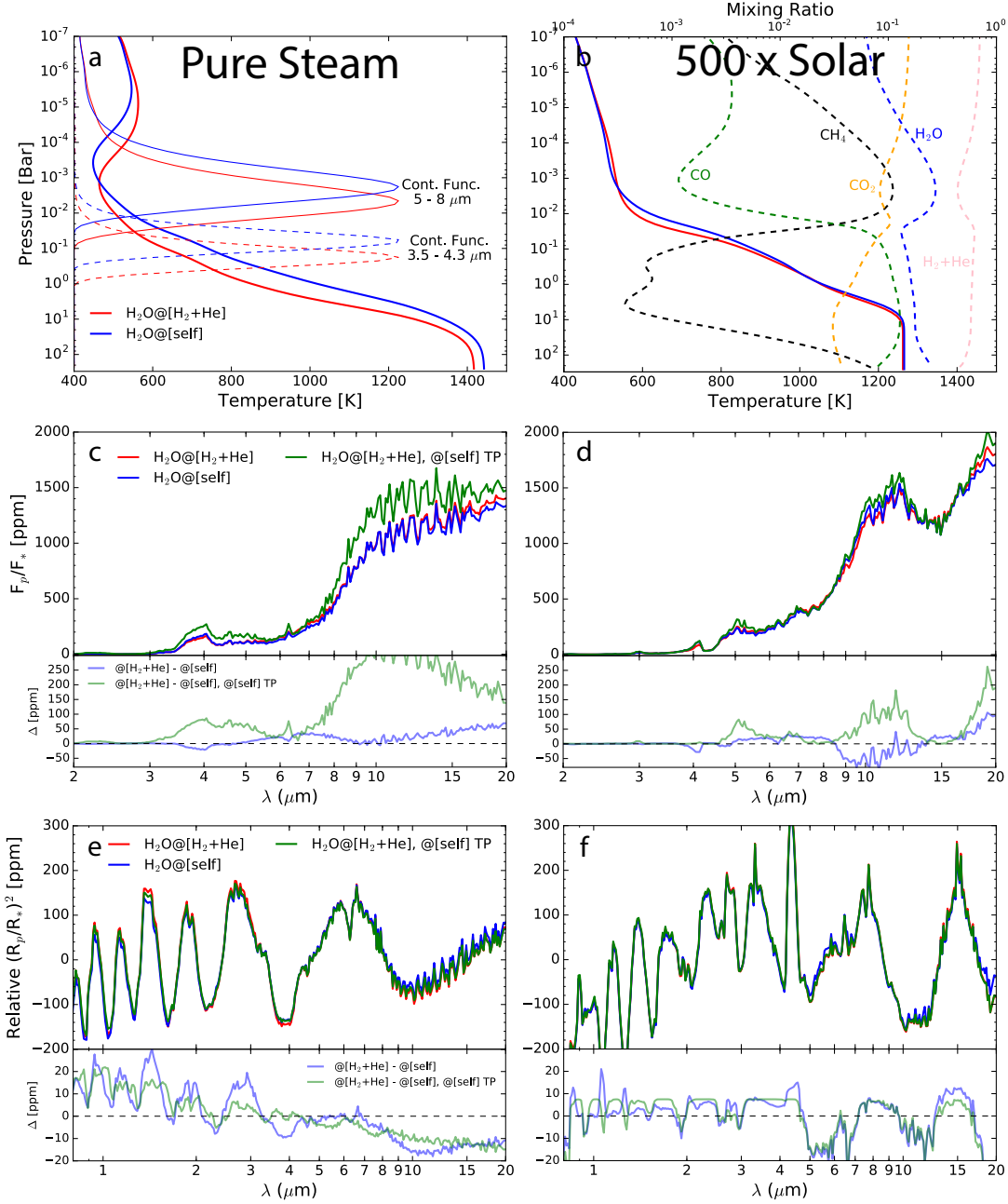


Figure 4. Comparison of the @self (blue) versus @[H₂+He] (red) broadening in self-consistent 1D thermochemical-radiative-equilibrium atmospheres for all steam (left column: a,c,e) and 500×solar (right column: b,d,f) composition. The top row (a,b) shows the derived radiative-equilibrium TP under each scenario. Thermal emission contribution functions averaged over representative bands (Cont. Func. 5–8, and 3.5–4.3 μm) for each broadening scenario are shown in (a). Subplot (b) shows the thermochemical equilibrium mixing ratios along the @self TP for select species. Temperature differences can be up to 175K (20%) in the pure steam scenario and up to 70K in the 500×Solar scenario. The second row (c,d) shows the resultant secondary eclipse spectra and their differences below (Δ). An additional emission spectrum (@[H₂+He], @[self] TP-green), is shown in (c) and (d) assuming the same TP as the @self scenario in order to decouple the effects of the radiatively adjusted TP from the broadening differences. The last row (e,f) shows the resulting cloud free transmission spectra and relative differences. An additional transmission spectrum (@[H₂+He], @[self] TP-green), is shown in (e) and (f) assuming the same TP as the @self scenario in order to decouple the effects of the broadening and scale height change due to TP variation. Spectral differences are on the order of 30–40 ppm in transmission but are much less in emission (~60 ppm) when compared to Figure 3a,b due to the radiative adjustment of the TP.

and ASU Research Computing center for the kind sup-

port on computational side. MRL acknowledges sum-

mer support from the NASA Exoplanet Research Program award NNX17AB56G. This work benefited from numerous conversations at the 2018 Exoplanet Summer

Program in the Other Worlds Laboratory (OWL) at the University of California, Santa Cruz, a program funded by the Heising-Simons Foundation.

REFERENCES

- Amundsen, D. S., Mayne, N. J., Baraffe, I., et al. 2016, *A & A*, 595, A36
- Arcangeli, J., Désert, J.-M., Line, M. R., et al. 2018, *ApJ*, 855, L30
- Barber, R. J., Tennyson, J., Harris, G. J., & Tolchenov, R. N. 2006, *MNRAS*, 368, 1087
- Barclay, T., Pepper, J., & Quintana, E. V. 2018, *ArXiv e-prints*, arXiv:1804.05050
- Barton, E. J., Hill, C., Yurchenko, S. N., et al. 2017, *JQSRT*, 187, 453
- Batalha, N. M. 2014, *PNAS*, 111, 12647
- Bean, J. L., Stevenson, K. B., Batalha, N. M., et al. 2018, *arXiv:1803.04985*
- Borucki, W. J., Koch, D. G., Dunham, E. W., & Jenkins, J. M. 1997, in *ASP Conf. Ser.*, Vol. 119, *Planets Beyond the Solar System and the Next Generation of Space Missions*, ed. D. Soderblom, 153
- Brown, L. R., Chris Benner, D., Malathy Devi, V., Smith, M. A., & Toth, R. A. 2005, *J. Molec. Struc.*, 742, 111
- Cridland, A. J., Pudritz, R. E., & Alessi, M. 2016, *MNRAS*, 461, 3274
- Delahaye, T., Landsheere, X., Pangui, E., et al. 2016a, *JQSRT*, 173, 40
- . 2016b, *JMS*, 326, 17
- Devi, M. V., Benner, C. D., Smith, M., et al. 2012, *JQSRT*, 113, 1013
- Devi, V. M., Benner, D. C., Smith, M. A., Rinsland, C. P., & Mantz, A. W. 2002, *JQSRT*, 75, 455
- Devi, V. M., Benner, D. C., Sung, K., et al. 2016, *JQSRT*, 177, 152
- Fortney, J. J., Mordasini, C., Nettelmann, N., et al. 2013, *ApJ*, 775, 80
- Fortney, J. J., Robinson, T. D., Domagal-Goldman, S., et al. 2016, *arXiv:1602.06305*
- Fraine, J., Deming, D., Benneke, B., et al. 2014, *Nature*, 513, 526
- Freedman, R. S., Lustig-Yaeger, J., Fortney, J. J., et al. 2014, *ApJS*, 214, 25
- Freedman, R. S., Marley, M. S., & Lodders, K. 2008, *ApJS*, 174, 504
- Fressin, F., Torres, G., Charbonneau, D., et al. 2013, *ApJ*, 766, 81
- Fulton, B. J., Petigura, E. A., Howard, A. W., et al. 2017, *AJ*, 154, 109
- Goody, R. M., & Yung, Y. L. 1995, *Atmospheric Radiation : Theoretical Basis.*, 2nd edn. (Oxford University Press), 536
- Gordon, I., Rothman, L., Hill, C., et al. 2017, *JQSRT*, 203, 3
- Gordon, S., & McBride, B. J. 1994, *Technical Report*
- Greene, T. P., Line, M. R., Montero, C., et al. 2016, *ApJ*, 817, 17
- Grimm, S. L., & Heng, K. 2015, *ApJ*, 808, 182
- Guillot, T. 2010, *A&A*, 520, A27
- Harpsøe, K. B. W., Hardis, S., Hinse, T. C., et al. 2013, *A&A*, 549, A10
- Hartmann, J. M., Rosenmann, L., Perrin, M. Y., & Taine, J. 1988, *App. Opt.*, 27, 3063
- Hartmann, J.-M., Tran, H., Armante, R., et al. 2018, *JQSRT*, 213, 178
- Hedges, C., & Madhusudhan, N. 2016, *MNRAS*, 458, 1427
- Hu, R., & Seager, S. 2014, *ApJ*, 784, 63
- Humlíček, J. 1979, *JQSRT*, 21, 309
- Kataria, T., Showman, A. P., Fortney, J. J., Marley, M. S., & Freedman, R. S. 2014, *ApJ*, 785, 92
- Kempton, E. M.-R., Bean, J. L., Louie, D. R., et al. 2018, *ArXiv e-prints*, arXiv:1805.03671
- Knutson, H. A., Benneke, B., Deming, D., & Homeier, D. 2014, *Nature*, 505, 66
- Kreidberg, L., Line, M. R., Thorngren, D., Morley, C. V., & Stevenson, K. B. 2018, *ApJ*, 858, L6
- Kreidberg, L., Bean, J. L., Désert, J.-M., et al. 2014a, *Nature*, 505, 69
- Kreidberg, L., Bean, J. L., Désert, J. M., et al. 2014b, *ApJL*, 793, 2
- Kreidberg, L., Line, M. R., Bean, J. L., et al. 2015, *ApJ*, 814, 66
- Line, M. R., Knutson, H., Deming, D., Wilkins, A., & Désert, J.-M. 2013, *ApJ*, 778, 183
- Line, M. R., Knutson, H., Wolf, A. S., & Yung, Y. L. 2014, *ApJ*, 783, 70
- Line, M. R., & Parmentier, V. 2016, *ApJ*, 820, 78
- Lodders, K., Palme, H., & Gail, H.-P. 2009, 712–770
- Lopez, E. D., & Fortney, J. J. 2014, *ApJ*, 792, 1
- Louie, D. R., Deming, D., Albert, L., et al. 2018, *PASP*, 130, 044401
- Lyons, J., Herde, H., Stark, G., et al. 2018, *JQSRT*, 210, 156

- Lyulin, O. M., Petrova, T. M., Solodov, A. M., Solodov, A. A., & Perevalov, V. I. 2014, *JQSRT*, 147, 164
- Madhusudhan, N., Agúndez, M., Moses, J. I., & Hu, Y. 2016, *Space Sci. Rev.*, 205, 285
- Madhusudhan, N., Amin, M. A., & Kennedy, G. M. 2014, *ApJL*, arXiv:1408.3668
- Mansfield, M., Bean, J. L., Line, M. R., et al. 2018, *AJ*, 156, 10
- Mihalas, D. 1970, *Series of Books in Astronomy and Astrophysics*, San Francisco: Freeman, —c1970
- Mordasini, C., van Boekel, R., Mollière, P., Henning, T., & Benneke, B. 2016, *ApJ*, 832, 1
- Morley, C. V., Knutson, H., Line, M., et al. 2017, *AJ*, 153, 86
- Moses, J. I. 2014, *Phil. Trans. Roy. Soc. A*, 372, 20130073
- Moses, J. I., Line, M. R., Visscher, C., et al. 2013, *ApJ*, 777, 34
- Öberg, K. I., Murray-Clay, R., & Bergin, E. A. 2011, *ApJL*, 743, L16
- Ohno, K., & Okuzumi, S. 2018, *ApJ*, 859, 34
- Olivero, J., & Longbothum, R. 1977, *JQSRT*, 17, 233
- Padmanabhan, A., Tzanetakis, T., Chanda, A., & Thomson, M. 2014, *JQSRT*, 133, 81
- Partridge, H., & Schwenke, D. W. 1997, *JCP*, 106, 4618
- Pine, A. S., & Gabard, T. 2003, *JMS*, 217, 105
- Pollack, J. B., Hubickyj, O., Bodenheimer, P., et al. 1996, *Icarus*, 124, 62
- Polyansky, O. L., Ovsyannikov, R. I., Kyuberis, A. A., et al. 2016, *JMS*, 327, 21
- Ptashnik, I. V., McPheat, R., Polyansky, O. L., Shine, K. P., & Smith, K. M. 2016, *JQSRT*, 177, 92
- Rothman, L., Rinsland, C., Goldman, A., et al. 1998, *JQSRT*, 60, 665
- Rothman, L., Gordon, I., Barber, R., et al. 2010, *JQSRT*, 111, 2139
- Smith, M. A., Benner, D. C., Predoi-Cross, A., & Malathy Devi, V. 2014, *JQSRT*, 133, 217
- Stevenson, K. B., Bean, J. L., Seifahrt, A., et al. 2014, *AJ*, 147, 161
- Sullivan, P. W., Winn, J. N., Berta-Thompson, Z. K., et al. 2015, *ApJ*, 809, 77
- Tennyson, J., Yurchenko, S. N., Al-Refaie, A. F., et al. 2016, *JMS*, 327, 73
- Yurchenko, S. N., Al-Refaie, A. F., & Tennyson, J. 2018, *A&A*, 614, A131